

MIMO Multipath-based SLAM for Non-Ideal Reflective Surfaces

Lukas Wielandner^{*†}, Alexander Venus^{*†}, Thomas Wilding^{*†}, Klaus Witrisal^{*†}, and Erik Leitinger^{*†}

^{*} Graz University of Technology, [†] Christian Doppler Laboratory for Location-Aware Electronic Systems
(e-mail: (lukas.wielandner, a.venus, thomas.wilding, witrisal, erik.leitinger)@tugraz.at)

Abstract—Multipath-based simultaneous localization and mapping (MP-SLAM) is a well established approach to obtain position information of transmitters and receivers as well as information regarding the propagation environments in future multiple input multiple output (MIMO) communication systems. Conventional methods for MP-SLAM consider specular reflections of the radio signals occurring at smooth, flat surfaces, which are modeled by virtual anchors (VAs) that are mirror images of the physical anchors (PAs), with each VA generating a single multipath component (MPC). However, non-ideal reflective surfaces (such as walls covered by shelves or cupboards) cause dispersion effects that violate the VA model and lead to multiple MPCs that are associated to a single VA. In this paper, we introduce a Bayesian particle-based sum-product algorithm (SPA) for MP-SLAM in MIMO communications systems. Our method considers non-ideal reflective surfaces by jointly estimating the parameters of individual dispersion models for each detected surface in delay and angle domain leveraging multiple-measurement-to-feature data association. We demonstrate that the proposed SLAM method can robustly and jointly estimate the positions and dispersion extents of ideal and non-ideal reflective surfaces using numerical simulation.

I. INTRODUCTION

Multipath-based simultaneous localization and mapping (MP-SLAM) is a promising approach to obtain position information of transmitters and receivers as well as information regarding their propagation environments in future mobile communication systems. Usually, specular reflections of radio signals at flat surfaces are modeled by virtual anchors (VAs) that are mirror images of the physical anchors (PAs) [1]–[4]. The positions of these VAs are unknown. MP-SLAM algorithms can detect and localize VAs and jointly estimate the unknown and time-varying position of mobile agents equipped with transmit or receive antennas [3]–[5]. The availability of VA location information makes it possible to leverage multipath propagation of radio signals for the localization of the mobile agent and can thus significantly improve its localization accuracy and robustness.

A. State of the Art

The proposed algorithm follows the feature-based simultaneous localization and mapping (SLAM) approach [6], [7], i.e., the map is represented by an unknown number of *map features*, whose unknown positions are estimated in a sequential (time-recursive) manner. Existing MP-SLAM algorithms consider VAs [3], [4], [8]–[10] or master VAs (MVs) [11], [12] as features to be mapped. Most of these methods use estimated parameters related to multipath

components (MPCs) contained in the radio signal, such as distances (which are proportional to delays), angle-of-arrivals (AOAs), or angle-of-departures (AODs) [4]. These parameters are estimated from the signal in a preprocessing stage [13]–[16] and are used as “measurements” available to the SLAM algorithm. Complicating factors in feature-based SLAM are measurement origin uncertainty, i.e., the unknown association of measurements with map features, and the time-varying and unknown number of map features. State-of-the-art methods for MP-SLAM are Bayesian estimators that consider these challenges in their joint statistical model leveraging probabilistic data association and the new potential object model [3], [4], [8], [15], [17]. These methods perform the sum-product algorithm (SPA) on the factor graph representing the resulting high dimensional estimation problem [3], [4], [8].

However, conventional MP-SLAM methods are prone to fail in scenarios with non-ideal reflective surfaces [18], [19] that violate the VA model. Such scenarios lead to *dispersion effects* (delay dispersion, angular dispersion) in the resulting radio signals. Furthermore, conventional MP-SLAM methods [3], [4], [8]–[10] assume a feature to generate only a single measurement (point object assumption) [3], [8], while the discussed dispersion effects can cause multiple measurements related to a single feature. In [20], we proposed a method that models the discussed dispersion effects by combining the VA model with a uniform dispersion model in delay domain by leveraging multiple-measurement-to-feature data association (developed for extended object tracking [17]) for MP-SLAM. This method can capture imperfections, such as caused by non-calibrated antennas, that result in similar dispersion effects over all map features. However, in realistic scenarios, one often faces varying dispersion effects for individual VAs due to rough walls [18], [19] or walls with cupboards or shelves.

B. Contributions

In this paper, we introduce a Bayesian particle-based SPA for MP-SLAM with non-ideal reflective surfaces. Based on the method from [20], [21], we model non-ideal reflective surfaces by capturing the resulting dispersion effects in measurement domain via a uniform dispersion extent model and probabilistic multiple-measurement-to-feature association [17], [22]. Different to [20], [21], the proposed algorithm can handle varying dispersion for individual map features by jointly inferring dedicated dispersion parameters for each PA and VA. Furthermore, we extend the work to multiple input multiple output (MIMO) systems by considering amplitude, delay, AOA, and AOD measurements and introducing a novel angular dispersion model, which is captured by jointly inferred angular dispersion parameters. Hence allowing us to treat

This work was supported in part by the Christian Doppler Research Association; the Austrian Federal Ministry for Digital and Economic Affairs; the National Foundation for Research, Technology, and Development. The project has received funding from the European Union’s Horizon 2020 research and innovation programme under grant agreement No 101013425.

(nearly) ideal surfaces as well as non-ideal (rough) surfaces in MIMO setups. The key contributions are as follows.

- We use individual dispersion parameters for each VA to account for the individual non-ideal reflective surfaces.
- We extend the work presented in [20], [21] to MIMO systems according to [4].
- We demonstrate based on synthetically generated measurements that the proposed SLAM method robustly associates single and multiple measurements per VA, hence allowing it to easily treat perfect reflectors (point objects) and rough surfaces (extended objects) in the same manner due to the likelihood function introduced in [20].

Notation: Random variables are displayed in sans serif, upright fonts; their realizations in serif, italic fonts. Vectors and matrices are denoted by bold lowercase and uppercase letters, respectively. For example, a random variable and its realization are denoted by \mathbf{x} and x , respectively, and a random vector and its realization by \mathbf{x} and \mathbf{x} , respectively. Furthermore, $\|\mathbf{x}\|$ and \mathbf{x}^T denote the Euclidean norm and the transpose of vector \mathbf{x} , respectively; \propto indicates equality up to a normalization factor; $f(\mathbf{x})$ denotes the probability density function (PDF) of random vector \mathbf{x} ; $f(\mathbf{x}|\mathbf{y})$ denotes the conditional PDF of random vector \mathbf{x} conditioned on random vector \mathbf{y} . $\delta(\cdot)$ denotes the Dirac delta function. $\text{atan2}(p_y, p_x)$ denotes the four quadrant inverse tangent of a vector $\mathbf{p} = [p_x \ p_y]^T$. The Gaussian PDF with respect to \mathbf{x} is $f_N(\mathbf{x}; \mu, \sigma) = \frac{1}{\sqrt{2\pi}\sigma} e^{-\frac{(\mathbf{x}-\mu)^2}{2\sigma^2}}$ with mean μ and standard deviation σ [23]. The Gamma PDF with respect to \mathbf{x} is denoted as $\mathcal{G}(\mathbf{x}; \alpha, \beta) = \frac{1}{\beta^\alpha \Gamma(\alpha)} x^{\alpha-1} e^{-\frac{x}{\beta}}$ where α is the shape parameter, β is the scale parameter and $\Gamma(\cdot)$ is the gamma-function. Finally, we define the uniform PDF $f_U(\mathbf{x}; a, b) = 1/(b-a)1_{[a,b]}(\mathbf{x})$.

II. GEOMETRICAL RELATIONS

At each time n , we consider a mobile agent with state $\mathbf{x}_n = [\mathbf{p}_n^T \ \mathbf{v}_n^T]^T$ at position $\mathbf{p}_n = [p_{x,n} \ p_{y,n}]^T$ moving with velocity $\mathbf{v}_n = [v_{x,n} \ v_{y,n}]^T$, and J base stations, called PAs, at known positions $\mathbf{p}_{\text{pa}}^{(j)} = [p_{x,\text{pa}}^{(j)} \ p_{y,\text{pa}}^{(j)}]^T \in \mathbb{R}^2$, $j \in \{1, \dots, J\}$, where J is assumed to be known, in an environment described by reflective surfaces. Both the agent and all PAs are equipped with antenna arrays. The geometry of an antenna array is represented by its array element positions, which are defined for the PAs arrays by the distances $d_{\text{ant}}^{(j,h)}$ and the angles $\psi_{\text{ant}}^{(j,h)}$ relative to the PA position $\mathbf{p}_{\text{pa}}^{(j)}$ (with known orientation), and for agent array by distance $d_{\text{ant}}^{(h)}$ and angle $\psi_{\text{ant}}^{(h)}$ relative to the agent position \mathbf{p}_n and unknown orientation κ_n . We assume that the agent array is rigidly coupled with \mathbf{v}_n , i.e., the array orientation is given as $\kappa_n = \text{atan2}(v_{y,n}, v_{x,n})$.

Specular reflections of radio signals at flat surfaces are modeled by VAs at positions $\mathbf{p}_{l,\text{va}}^{(j)} = [p_{x,l,\text{va}}^{(j)} \ p_{y,l,\text{va}}^{(j)}]^T$ that are mirror images of PAs (for details see [12]). The according point of reflection $\mathbf{q}_{l,n}^{(j)}$ at the surface is given as

$$\mathbf{q}_{l,n}^{(j)} = \mathbf{p}_{l,\text{va}}^{(j)} + \frac{(\mathbf{p}_{\text{pa}}^{(j)} - \mathbf{p}_{l,\text{va}}^{(j)})^T \mathbf{u}_l}{2(\mathbf{p}_n - \mathbf{p}_{l,\text{va}}^{(j)})^T \mathbf{u}_l} (\mathbf{p}_n - \mathbf{p}_{l,\text{va}}^{(j)}) \quad (1)$$

where \mathbf{u}_l is the normal vector of the according reflective surface. The point of reflection is needed to relate AOD

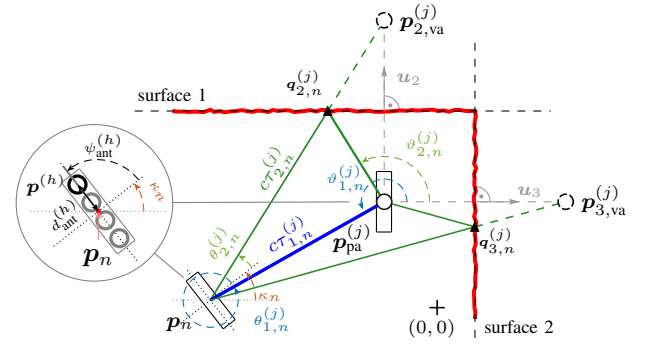


Fig. 1. Exemplary indoor environment including an agent at position \mathbf{p}_n , a PA at position $\mathbf{p}_{\text{pa}}^{(j)}$ and two VAs at positions $\mathbf{p}_{l,\text{va}}^{(j)}$ for corresponding surfaces. A visualization of the array geometry definition used at the agent and PAs is included.

measurements of MPCs to the corresponding VA. An example is shown in Fig. 1. Since we are using AOD measurements and VAs as map features, we can only consider VAs associated with a single-bounce path within the algorithm. An extension to multiple-bounce path is possible using the MVAs model [12]. The current number of *visible* VAs within the scenario is $L_n^{(j)}$ for each of the J PAs. A VA does not exist at time n , when the path between the agent and this VA is obstructed.

III. RADIO SIGNAL MODEL

At each time n , the mobile agent transmits a signal $s(t)$ from an antenna array equipped with H antenna elements and each PA $j \in \{1, \dots, J\}$ acts as a receiver equipped with an array with $H^{(j)}$ antenna elements. In the following, we define $\mathbf{p}_{1,\text{va}}^{(j)} \triangleq \mathbf{p}_{\text{pa}}^{(j)}$. The received complex baseband signal at the j th PA is sampled with sampling frequency $f_s = 1/T_s = B$, giving an observation period of $T = N_s T_s$. Stacking these N_s samples, we obtain the discrete received signal vector in frequency domain between antenna elements h at the agent and h' at PA j as [20], [24]

$$\begin{aligned} \mathbf{s}_{\text{rx},n}^{(j)}[h, h'] &= \sum_{l=1}^{L_n^{(j)}} \sum_{i=1}^{L_{l,n}^{(j)}} \alpha_{l,i,n}^{(j)} \exp(i2\pi \frac{f_c}{c} d_{\text{ant}}^{(h)} \cos(\theta_{l,i,n}^{(j)} - \psi_{\text{ant}}^{(h)})) \\ &\quad \times \exp(i2\pi \frac{f_c}{c} d_{\text{ant}}^{(j,h')} \cos(\vartheta_{l,i,n}^{(j)} - \psi_{\text{ant}}^{(j,h')})) \\ &\quad \times \mathbf{s}(\tau_{l,i,n}^{(j)}) + \mathbf{w}_n^{(j)}[h, h'] \end{aligned} \quad (2)$$

where $[\mathbf{s}(\tau)]_\ell = S(\ell\Delta) \exp(i2\pi\ell\Delta\tau)$ is the ℓ th frequency sample of the signal spectrum $S(f)$ and c is the speed of light. The parameters of the l th MPC at the agent and the j th PA (for $l = 1$) or the corresponding VAs (for $l \in \{2, \dots, L_n^{(j)}\}$) are the complex amplitude $\alpha_{l,i,n}^{(j)} \in \mathbb{C}$, the delay $\tau_{l,i,n}^{(j)} = \tau(\mathbf{p}_n, \mathbf{p}_{l,\text{va}}^{(j)}) + \nu_{l,i,n}^{(j)}$ with $\tau(\mathbf{p}_n, \mathbf{p}_{l,\text{va}}^{(j)}) \triangleq \|\mathbf{p}_n - \mathbf{p}_{l,\text{va}}^{(j)}\|/c$, the AOA $\theta_{l,i,n}^{(j)} = \theta(\mathbf{x}_n, \mathbf{p}_{l,\text{va}}^{(j)}) + \eta_{l,i,n}^{(j)}$ with $\theta(\mathbf{x}_n, \mathbf{p}_{l,\text{va}}^{(j)}) \triangleq \text{atan2}(p_{y,l,\text{va}}^{(j)} - p_{y,n}, p_{x,l,\text{va}}^{(j)} - p_{x,n}) - \kappa_n$, and AOD $\vartheta_{l,i,n}^{(j)} = \vartheta(\mathbf{p}_n, \mathbf{p}_{l,\text{va}}^{(j)}) + \zeta_{l,i,n}^{(j)}$. For AOD, we have to distinguish between $\vartheta(\mathbf{p}_n, \mathbf{p}_{\text{pa}}^{(j)}) \triangleq \text{atan2}(p_{y,n} - p_{y,\text{pa}}^{(j)}, p_{x,n} - p_{x,\text{pa}}^{(j)})$ for $l = 1$ and $\vartheta(\mathbf{p}_n, \mathbf{p}_{l,\text{va}}^{(j)}) \triangleq \text{atan2}(q_{y,l,n}^{(j)} - p_{y,n}, q_{x,l,n}^{(j)} - p_{x,n})$ for $l \neq 1$, where $\mathbf{q}_{l,n}^{(j)}$ is calculated based on (1) using \mathbf{p}_n .

Due to the effects of non-ideal reflective surfaces, there are $L_{l,n}^{(j)}$ sub-components associated to the l th MPC generated

by a marked Poisson point process [20], [24], [25]. Note that with the intensity distribution of the complex amplitudes $\alpha_{l,i,n}^{(j)}$ and arrival distributions of the sub-components in delay $\nu_{l,i,n}^{(j)}$, in AOA $\eta_{l,i,n}^{(j)}$, and in AOD $\zeta_{l,i,n}^{(j)}$ many different non-ideal effects of surfaces such as roughness [18], [19] can be described. However, for the sake of simplicity and effectiveness, we have chosen the following simple model. We assume that for each MPC l there is a main-component $i = 1$ and the $L_{l,n}^{(j)} - 1$ sub-components with index $i \in \{2, \dots, L_{l,n}^{(j)}\}$. The main-component is described by the complex amplitude $\alpha_{l,1,n}^{(j)} \in \mathbb{C}$, the delay $\tau_{l,1,n}^{(j)} = \tau(\mathbf{p}_n, \mathbf{p}_{l,va}^{(j)})$, the AOA $\theta_{l,1,n}^{(j)} = \theta(\mathbf{x}_n, \mathbf{p}_{l,va}^{(j)})$, and AOD $\vartheta_{l,1,n}^{(j)} = \vartheta(\mathbf{p}_n, \mathbf{p}_{l,va}^{(j)})$. The sub-components are assumed to have complex amplitudes $\alpha_{l,i,n}^{(j)} = \alpha_{l,1,n}^{(j)} \beta_{l,i,n}$ with attenuation $\beta_{l,i,n}$ and to be uniformly distributed over the dispersion domains $\nu_{l,i,n}^{(j)} \in [0, \psi_{\tau,l,n}^{(j)}]$, $\eta_{l,i,n}^{(j)} \in [-\psi_{\theta,l,n}^{(j)}/2, \psi_{\theta,l,n}^{(j)}/2]$, and $\zeta_{l,i,n}^{(j)} \in [-\psi_{\vartheta,l,n}^{(j)}/2, \psi_{\vartheta,l,n}^{(j)}/2]$, where $\psi_{\tau,l,n}^{(j)}$, $\psi_{\theta,l,n}^{(j)}$, and $\psi_{\vartheta,l,n}^{(j)}$ are called dispersion parameters. Note that the distributions of these parameters will depend on the environment properties and can vary per component and PA.

The noise vector $\mathbf{w}_n^{(j)}[h, h'] \in \mathbb{C}^{N_s}$ is a zero-mean, circularly-symmetric complex Gaussian random vector with covariance matrix $\sigma^{(j)2} \mathbf{I}_{N_s} \forall h, h'$ and noise variance $\sigma^{(j)2}$.

A. Parametric Channel Estimation

By applying at each time n , a channel estimation and detection algorithm (CEDA) [13]–[16] to the full observed discrete signal vector $\mathbf{s}_{rx,n}^{(j)} = [\mathbf{s}_{rx,n}^{(j)}[1, 1]^T \dots \mathbf{s}_{rx,n}^{(j)}[H, H^{(j)}]^T]^T \in \mathbb{C}^{NH^{(j)}}$ of all antenna elements at agent and PA j , one obtains, for each PA j , a number of $M_n^{(j)}$ measurements denoted by $\mathbf{z}_{m,n}^{(j)}$ with $m \in \mathcal{M}_n^{(j)} \triangleq \{1, \dots, M_n^{(j)}\}$. Each $\mathbf{z}_{m,n}^{(j)} = [z_{\tau,m,n}^{(j)} \ z_{\theta,m,n}^{(j)} \ z_{\vartheta,m,n}^{(j)} \ z_{u,m,n}^{(j)}]^T$ representing a potential MPC parameter estimate, contains a delay measurement $z_{\tau,m,n}^{(j)} \in [0, \tau_{\max}]$ an AOA measurement $z_{\theta,m,n}^{(j)} \in [-\pi, \pi]$ and an AOD measurement $z_{\vartheta,m,n}^{(j)} \in [-\pi, \pi]$. We also get a normalized amplitude measurement¹ $z_{u,m,n}^{(j)} \in [\gamma, \infty)$, where γ is the detection threshold. The CEDA decomposes the signal $\mathbf{s}_{rx,n}^{(j)}$ into individual, decorrelated components reducing significantly the number of dimensions ($M_n^{(j)} \ll N_s H H'$). It thus compresses the information contained in $\mathbf{s}_{rx,n}^{(j)}$ into $\mathbf{z}_n^{(j)} = [\mathbf{z}_{1,n}^{(j)T} \dots \mathbf{z}_{M_n^{(j)},n}^{(j)T}]^T$. The stacked vector $\mathbf{z}_n = [\mathbf{z}_n^{(1)T} \dots \mathbf{z}_n^{(J)T}]^T$ is used by the proposed algorithm as a noisy measurement.

IV. SYSTEM MODEL

At each time n , the state $\mathbf{x}_n = [\mathbf{p}_n^T \ \mathbf{v}_n^T]^T$ of the agent consists of its position \mathbf{p}_n and velocity \mathbf{v}_n . In line with [8], [15], [26], we account for the unknown number of VAs by introducing for each PA j potential VAs (PVAs) $k \in \mathcal{K}_n^{(j)} \triangleq \{1, \dots, K_n^{(j)}\}$. The number of PVAs $K_n^{(j)}$ is

¹The normalized amplitude measurements are determined as $z_{u,m,n}^{(j)} = |\mu_{\alpha,m,n}^{(j)}|/\sigma_{\alpha,m,n}^{(j)}$ with $\mu_{\alpha,m,n}^{(j)} \in \mathbb{C}$ and $\sigma_{\alpha,m,n}^{(j)} \in \mathbb{R}^+$ denoting respectively the estimated mean and standard deviation of the complex amplitudes provided by the CEDA.

the maximum possible number of VAs of PA j that produced measurements so far [26] (i.e., $K_n^{(j)}$ increases with time). The state of PVA (j, k) is denoted as $\mathbf{y}_{k,n}^{(j)} \triangleq [\mathbf{x}_{k,n}^{(j)T} \ r_{k,n}^{(j)}]^T$ with $\mathbf{x}_{k,n}^{(j)} = [\mathbf{p}_{k,va}^{(j)T} \ \boldsymbol{\psi}_{k,n}^{(j)T}]^T$, which includes the dispersion parameters $\boldsymbol{\psi}_{k,n}^{(j)} = [\psi_{\tau,k,n}^{(j)} \ \psi_{\theta,k,n}^{(j)} \ \psi_{\vartheta,k,n}^{(j)}]^T$. The existence/nonexistence of PVA k is modeled by the existence variable $r_{k,n}^{(j)} \in \{0, 1\}$ in the sense that PVA k exists if and only if $r_{k,n}^{(j)} = 1$. The PVA state is considered formally also if PVA k is nonexistent, i.e., if $r_{k,n}^{(j)} = 0$. Since a part of the PA state is unknown, we also consider the PA itself a PVA. Hence, we distinguish between the PVA $k = 1$ that explicitly represents the PA, which is a-priori existent and has known (fixed) position $\mathbf{p}_{1,va}^{(j)} = \mathbf{p}_{pa}^{(j)}$, and all other PVAs $k \in \{2, \dots, K_n^{(j)}\}$ with unknown existences and positions. Note that the PVAs state representing the PA still considers the existence variable $r_{1,n}^{(j)}$. The states $\mathbf{x}_{k,n}^{(j)}$ of nonexistent PVAs are obviously irrelevant. Therefore, all PDFs defined for PVA states, $f(\mathbf{y}_{k,n}^{(j)}) = f(\mathbf{x}_{k,n}^{(j)}, r_{k,n}^{(j)})$, are of the form $f(\mathbf{x}_{k,n}^{(j)}, 0) = f_{k,n}^{(j)} f_d(\mathbf{x}_{k,n}^{(j)})$, where $f_d(\mathbf{x}_{k,n}^{(j)})$ is an arbitrary “dummy” PDF and $f_{k,n}^{(j)} \in [0, 1]$ is a constant. We also define the stacked vectors $\mathbf{y}_n^{(j)} \triangleq [\mathbf{y}_{1,n}^{(j)T} \dots \mathbf{y}_{K_n^{(j)},n}^{(j)T}]^T$ and $\mathbf{y}_n \triangleq [\mathbf{y}_n^{(1)T} \dots \mathbf{y}_n^{(J)T}]^T$.

A. State Evolution

For each PVA with state $\mathbf{y}_{k,n-1}^{(j)}$ with $k \in \mathcal{K}_{n-1}^{(j)} \triangleq \{1, \dots, K_{n-1}^{(j)}\}$ at time $n-1$ and PA j , there is one “legacy” PVA with state $\mathbf{y}_{k,n}^{(j)} \triangleq [\mathbf{x}_{k,n}^{(j)T} \ r_{k,n}^{(j)}]^T$ with $k \in \mathcal{K}_{n-1}^{(j)}$ at time n and PA j . We also define the joint states $\mathbf{y}_n^{(j)} \triangleq [\mathbf{y}_{1,n}^{(j)T} \dots \mathbf{y}_{K_{n-1}^{(j)},n}^{(j)T}]^T$ and $\mathbf{y}_n \triangleq [\mathbf{y}_n^{(1)T} \dots \mathbf{y}_n^{(J)T}]^T$. Assuming that the agent state as well as the PVA states of all PAs evolve independently across k , n , and j , the joint state-transition PDF factorizes as [3], [26]

$$f(\mathbf{x}_n, \mathbf{y}_n | \mathbf{x}_{n-1}, \mathbf{y}_{n-1}) = f(\mathbf{x}_n | \mathbf{x}_{n-1}) \prod_{j=1}^J \prod_{k=1}^{K_{n-1}^{(j)}} f(\mathbf{y}_{k,n}^{(j)} | \mathbf{y}_{k,n-1}^{(j)}) \quad (3)$$

where $f(\mathbf{y}_{k,n}^{(j)} | \mathbf{y}_{k,n-1}^{(j)}) \triangleq f(\mathbf{x}_{k,n}^{(j)}, r_{k,n}^{(j)} | \mathbf{x}_{k,n-1}^{(j)}, r_{k,n-1}^{(j)})$ is the legacy PVA state-transition PDF. If PVA did not exist at time $n-1$, i.e., $r_{k,n-1}^{(j)} = 0$, it cannot exist as a legacy PVA at time n either. Thus,

$$f(\mathbf{x}_{k,n}^{(j)}, r_{k,n}^{(j)} | \mathbf{x}_{k,n-1}^{(j)}, 0) = \begin{cases} f_d(\mathbf{x}_{k,n}^{(j)}), & r_{k,n}^{(j)} = 0 \\ 0, & r_{k,n}^{(j)} = 1. \end{cases} \quad (4)$$

If PVA existed at time $n-1$, i.e., $r_{k,n-1}^{(j)} = 1$, it either dies, i.e., $r_{k,n}^{(j)} = 0$, or survives, i.e., $r_{k,n}^{(j)} = 1$ with survival probability denoted as p_s . If it does survive, its state $\mathbf{y}_{k,n}^{(j)}$ is distributed according to the state-transition PDF $f(\mathbf{x}_{k,n}^{(j)} | \mathbf{x}_{k,n-1}^{(j)}) \triangleq \delta(\mathbf{p}_{k,va}^{(j)} - \mathbf{p}_{k,va}^{(j)}) f(\psi_{k,n}^{(j)} | \psi_{k,n-1}^{(j)})$ [3], [8]. Thus,

$$f(\mathbf{x}_{k,n}^{(j)}, r_{k,n}^{(j)} | \mathbf{x}_{k,n-1}^{(j)}, 1) = \begin{cases} (1-p_s) f_d(\mathbf{x}_{k,n}^{(j)}), & r_{k,n}^{(j)} = 0 \\ p_s \delta(\mathbf{p}_{k,va}^{(j)} - \mathbf{p}_{k,va}^{(j)}) f(\psi_{k,n}^{(j)} | \psi_{k,n-1}^{(j)}), & r_{k,n}^{(j)} = 1. \end{cases} \quad (5)$$

The agent state \mathbf{x}_n with state-transition PDF $f(\mathbf{x}_n | \mathbf{x}_{n-1})$ is assumed to evolve in time according to a 2-dimensional,

constant velocity and stochastic acceleration model [27] given as $\mathbf{x}_n = \mathbf{A}\mathbf{x}_{n-1} + \mathbf{B}\mathbf{w}_n$, with the acceleration process \mathbf{w}_n being independent and identically distributed (iid) across n , zero mean, and Gaussian with covariance matrix $\sigma_w^2 \mathbf{I}_2$, σ_w is the acceleration standard deviation, and $\mathbf{A} \in \mathbb{R}^{4 \times 4}$ and $\mathbf{B} \in \mathbb{R}^{4 \times 2}$ are defined according to [27, p. 273], with observation period ΔT . The state-transition PDFs of the dispersion parameter states $f(\psi_{k,n}^{(j)}|\psi_{k,n-1}^{(j)}) = f(\psi_{\tau,k,n}^{(j)}|\psi_{\tau,k,n-1}^{(j)})f(\psi_{\theta,k,n}^{(j)}|\psi_{\theta,k,n-1}^{(j)})f(\psi_{\vartheta,k,n}^{(j)}|\psi_{\vartheta,k,n-1}^{(j)})$ are assumed to evolve independently of each other across n . We model the individual state-transition PDFs by Gamma PDFs given respectively by $f(\psi_{\tau,k,n}^{(j)}|\psi_{\tau,k,n-1}^{(j)}) = \mathcal{G}(\psi_{\tau,k,n}^{(j)}; q_\tau, \psi_{\tau,k,n-1}^{(j)}/q_\tau)$, $f(\psi_{\theta,k,n}^{(j)}|\psi_{\theta,k,n-1}^{(j)}) = \mathcal{G}(\psi_{\theta,k,n}^{(j)}; q_\theta, \psi_{\theta,k,n-1}^{(j)}/q_\theta)$ and $f(\psi_{\vartheta,k,n}^{(j)}|\psi_{\vartheta,k,n-1}^{(j)}) = \mathcal{G}(\psi_{\vartheta,k,n}^{(j)}; q_\vartheta, \psi_{\vartheta,k,n-1}^{(j)}/q_\vartheta)$, where q_τ , q_θ and q_ϑ represent the respective state noise parameters [17], [28]. Small q implies a large state transition uncertainty.

B. Measurement Model

Before the measurements are observed, they are random and represented by the vector $\mathbf{z}_{m,n}^{(j)} = [z_{\tau m,n}^{(j)} z_{\theta m,n}^{(j)} z_{\vartheta m,n}^{(j)} z_{um,n}^{(j)}]^T$. In line with Section III-A we define the nested random vectors $\mathbf{z}_n^{(j)} = [\mathbf{z}_{1,n}^{(j)T} \dots \mathbf{z}_{M_n^{(j)},n}^{(j)T}]^T$, with length corresponding to the random number of measurements $M_n^{(j)}$, and $\mathbf{z}_n = [\mathbf{z}_n^{(1)T} \dots \mathbf{z}_n^{(J)T}]^T$. The vector containing all numbers of measurements is defined as $\mathbf{M}_n = [M_n^{(1)} \dots M_n^{(J)}]^T$.

If PVA k exists ($r_{k,n}^{(j)} = 1$), it gives rise to a random number of measurements. The mean number of measurements per (existing) PVA is modeled by a Poisson point process with mean $\mu_m(\psi_{k,n}^{(j)})$. The individual measurements $\mathbf{z}_{m,n}^{(j)}$ are assumed to be conditionally independent, i.e., the joint PDF of all measurements factorizes as $f(\mathbf{z}_n^{(j)}|\mathbf{M}_n^{(j)}, \mathbf{x}_n, \nu_{k,n}^{(j)}, \eta_{k,n}^{(j)}, \zeta_{k,n}^{(j)}, \mathbf{x}_{k,n}^{(j)}) = \prod_{m=1}^{M_n^{(j)}} f(z_{m,n}^{(j)}|\mathbf{x}_n, \nu_{k,n}^{(j)}, \eta_{k,n}^{(j)}, \zeta_{k,n}^{(j)}, \mathbf{x}_{k,n}^{(j)})$.

If $\mathbf{z}_{m,n}^{(j)}$ is generated by a PVA, i.e., it corresponds to a main-component (line-of-sight (LOS) component or MPC), we assume that the single-measurement likelihood function (LHF) $f(z_{m,n}^{(j)}|\mathbf{x}_n, \nu_{k,n}^{(j)}, \eta_{k,n}^{(j)}, \zeta_{k,n}^{(j)}, \mathbf{x}_{k,n}^{(j)})$ is conditionally independent across $z_{\tau m,n}^{(j)}$, $z_{\theta m,n}^{(j)}$ and $z_{\vartheta m,n}^{(j)}$. Thus, it factorizes as

$$f(z_{m,n}^{(j)}|\mathbf{x}_n, \nu_{k,n}^{(j)}, \eta_{k,n}^{(j)}, \zeta_{k,n}^{(j)}) = f(z_{\tau m,n}^{(j)}|\mathbf{x}_n, \nu_{k,n}^{(j)}) \times f(z_{\theta m,n}^{(j)}|\mathbf{x}_n, \eta_{k,n}^{(j)}) f(z_{\vartheta m,n}^{(j)}|\mathbf{x}_n, \zeta_{k,n}^{(j)}). \quad (6)$$

The LHF of the corresponding delay measurement $z_{\tau m,n}^{(j)}$ is given by

$$f(z_{\tau m,n}^{(j)}|\mathbf{p}_n, \mathbf{x}_{k,n}^{(j)}, \nu_{k,n}^{(j)}) = f_N(z_{\tau m,n}^{(j)}; \tau(\mathbf{p}_n, \mathbf{p}_{k,va}^{(j)}) + \nu_{k,n}^{(j)}, \sigma_\tau^2(z_{um,n}^{(j)})) \quad (7)$$

with mean $\tau(\mathbf{p}_n, \mathbf{p}_{k,va}^{(j)}) + \nu_{k,n}^{(j)}$ and variance $\sigma_\tau^2(z_{um,n}^{(j)})$. The standard deviation is determined from the Fisher information given by $\sigma_\tau^2(u) = c^2/(8\pi^2\beta_{bw}^2 u^2)$ with β_{bw} being the root mean squared bandwidth [29] (see Section V). The LHF of the corresponding AOA measurement $z_{\theta m,n}^{(j)}$ is obtained as

$$f(z_{\theta m,n}^{(j)}|\mathbf{x}_n, \mathbf{x}_{k,n}^{(j)}, \eta_{k,n}^{(j)})$$

$$= f_N(z_{\theta m,n}^{(j)}; \theta(\mathbf{x}_n, \mathbf{p}_{k,va}^{(j)}) + \eta_{k,n}^{(j)}, \sigma_\theta^2(z_{um,n}^{(j)})) \quad (8)$$

with mean $\theta(\mathbf{x}_n, \mathbf{p}_{k,va}^{(j)}) + \eta_{k,n}^{(j)}$ and variance $\sigma_\theta^2(z_{um,n}^{(j)})$ [29].

The LHF of the corresponding AOD measurement $z_{\vartheta m,n}^{(j)}$ is defined in a similar manner. Based on the dispersion model introduced in the Section III, the joint PDF of the dispersion variables can be constructed as follows [20]

$$f(\nu_{k,n}^{(j)}, \eta_{k,n}^{(j)}, \zeta_{k,n}^{(j)}|\psi_n^{(j)}) = \frac{1}{2} \left(\delta(\nu_{k,n}^{(j)}) \delta(\eta_{k,n}^{(j)}) \delta(\zeta_{k,n}^{(j)}) + \delta(\nu_{k,n}^{(j)} - \psi_{\tau,k,n}^{(j)}) \delta(\eta_{k,n}^{(j)} - \psi_{\theta,k,n}^{(j)}) \delta(\zeta_{k,n}^{(j)} - \psi_{\vartheta,k,n}^{(j)}) \right. \\ \times f_U(\nu_{k,n}^{(j)}; 0, \psi_{\tau,k,n}^{(j)}) f_U(\eta_{k,n}^{(j)}; -\psi_{\theta,k,n}^{(j)}/2, \psi_{\vartheta,k,n}^{(j)}/2) \\ \times f_U(\zeta_{k,n}^{(j)}; -\psi_{\vartheta,k,n}^{(j)}/2, \psi_{\theta,k,n}^{(j)}/2) \left. \right) \quad (9)$$

where the according delay dispersion random variable is given as $\nu_{k,n}^{(j)} \sim f_U(\nu_{k,n}^{(j)}; 0, \psi_{\tau,k,n}^{(j)})$ and the angular dispersion random variables are $\eta_{k,n}^{(j)} \sim f_U(\eta_{k,n}^{(j)}; -\psi_{\theta,k,n}^{(j)}/2, \psi_{\vartheta,k,n}^{(j)}/2)$ and $\zeta_{k,n}^{(j)} \sim f_U(\zeta_{k,n}^{(j)}; -\psi_{\vartheta,k,n}^{(j)}/2, \psi_{\theta,k,n}^{(j)}/2)$. The PDF of a single measurement $\mathbf{z}_{m,n}^{(j)}$ can now be obtained by integrating out the dispersion variables as

$$f(z_{m,n}^{(j)}|\mathbf{x}_n, \mathbf{x}_{k,n}^{(j)}) = \int f(z_{m,n}^{(j)}|\mathbf{x}_n, \mathbf{p}_{k,va}^{(j)}, \nu_{k,n}^{(j)}, \eta_{k,n}^{(j)}, \zeta_{k,n}^{(j)}) \\ \times f(\nu_{k,n}^{(j)}, \eta_{k,n}^{(j)}, \zeta_{k,n}^{(j)}|\psi_n^{(j)}) d\nu_{k,n}^{(j)} d\eta_{k,n}^{(j)} d\zeta_{k,n}^{(j)} \\ = f(z_{\tau m,n}^{(j)}|\mathbf{p}_n, \mathbf{p}_{k,va}^{(j)}) f(z_{\theta m,n}^{(j)}|\mathbf{x}_n, \mathbf{p}_{k,va}^{(j)}) f(z_{\vartheta m,n}^{(j)}|\mathbf{p}_n, \mathbf{p}_{k,va}^{(j)}) \\ + f(z_{\tau m,n}^{(j)}|\mathbf{p}_n, \mathbf{p}_{k,va}^{(j)}, \psi_{\tau,k}^{(j)}) f(z_{\theta m,n}^{(j)}|\mathbf{x}_n, \mathbf{p}_{k,va}^{(j)}, \psi_{\theta,k}^{(j)}) \\ \times f(z_{\vartheta m,n}^{(j)}|\mathbf{p}_n, \mathbf{p}_{k,va}^{(j)}, \psi_{\vartheta,k}^{(j)}) \quad (10)$$

with the main-component PDFs

$$f(z_{\tau m,n}^{(j)}|\mathbf{p}_n, \mathbf{p}_{k,va}^{(j)}) = f_N(z_{\tau m,n}^{(j)}; \tau(\mathbf{p}_n, \mathbf{p}_{k,va}^{(j)}), \sigma_\tau^2(z_{um,n}^{(j)})) \quad (11)$$

$$f(z_{\theta m,n}^{(j)}|\mathbf{x}_n, \mathbf{p}_{k,va}^{(j)}) = f_N(z_{\theta m,n}^{(j)}; \theta(\mathbf{x}_n, \mathbf{p}_{k,va}^{(j)}), \sigma_\theta^2(z_{um,n}^{(j)})) \quad (12)$$

$$f(z_{\vartheta m,n}^{(j)}|\mathbf{p}_n, \mathbf{p}_{k,va}^{(j)}) = f_N(z_{\vartheta m,n}^{(j)}; \vartheta(\mathbf{p}_n, \mathbf{p}_{k,va}^{(j)}), \sigma_\vartheta^2(z_{um,n}^{(j)})) \quad (13)$$

as well as the additional sub-component PDFs

$$f(z_{\tau m,n}^{(j)}|\mathbf{p}_n, \mathbf{p}_{k,va}^{(j)}, \psi_{\tau,n}^{(j)}) \\ = \frac{1}{\psi_{\tau,n}^{(j)}} \int_0^{\psi_{\tau,n}^{(j)}} f_N(z_{\tau m,n}^{(j)}; \tau(\mathbf{p}_n, \mathbf{p}_{k,va}^{(j)}) + \nu_{k,n}^{(j)}, \sigma_\tau^2(z_{um,n}^{(j)})) d\nu_{k,n}^{(j)} \\ = \frac{1}{2\psi_{\tau,n}^{(j)}} \left(\text{erf} \left(\frac{\tau(\mathbf{p}_n, \mathbf{p}_{k,va}^{(j)}) + \psi_{\tau,n}^{(j)} - z_{\tau m,n}^{(j)}}{\sigma_\tau(z_{um,n}^{(j)})\sqrt{2}} \right) \right. \\ \left. - \text{erf} \left(\frac{\tau(\mathbf{p}_n, \mathbf{p}_{k,va}^{(j)}) - z_{\tau m,n}^{(j)}}{\sigma_\tau(z_{um,n}^{(j)})\sqrt{2}} \right) \right) \quad (14)$$

and

$$f(z_{\theta m,n}^{(j)}|\mathbf{x}_n, \mathbf{p}_{k,va}^{(j)}, \psi_{\theta,n}^{(j)}) \\ = \frac{1}{\psi_{\theta,n}^{(j)}} \int_{-\psi_{\theta,n}^{(j)}/2}^{\psi_{\theta,n}^{(j)}/2} f_N(z_{\theta m,n}^{(j)}; \theta(\mathbf{x}_n, \mathbf{p}_{k,va}^{(j)}) + \eta_{k,n}^{(j)}, \sigma_\theta^2(z_{um,n}^{(j)})) d\eta_{k,n}^{(j)} \\ = \frac{1}{2\psi_{\theta,n}^{(j)}} \left(\text{erf} \left(\frac{\theta(\mathbf{x}_n, \mathbf{p}_{k,va}^{(j)}) + \psi_{\theta,n}^{(j)}/2 - z_{\theta m,n}^{(j)}}{\sigma_\theta(z_{um,n}^{(j)})\sqrt{2}} \right) \right. \\ \left. - \text{erf} \left(\frac{\theta(\mathbf{x}_n, \mathbf{p}_{k,va}^{(j)}) - \psi_{\theta,n}^{(j)}/2 - z_{\theta m,n}^{(j)}}{\sigma_\theta(z_{um,n}^{(j)})\sqrt{2}} \right) \right) \quad (15)$$

where $f(z_{\vartheta m,n}^{(j)} | \mathbf{p}_n, \mathbf{p}_{k,va}^{(j)}, \psi_{\vartheta,n}^{(j)})$ is defined in a similar manner as (15). Note that in (13), we have to distinguish between $k = 1$ and $k \neq 1$ (see Section III). It is also possible that a measurement $\mathbf{z}_{m,n}^{(j)}$ did not originate from any PVA (false positive measurements comprise false alarms and clutter measurements). False positive measurements are assumed statistically independent of PVA states. They are modeled by a Poisson point process with mean μ_{fp} and PDF $f_{fp}(z_{m,n}^{(j)})$, which is assumed to factorize as $f_{fp}(z_{m,n}^{(j)}) = f_{fp}(z_{\tau m,n}^{(j)}) f_{fp}(z_{\vartheta m,n}^{(j)}) f_{fp}(z_{\varphi m,n}^{(j)})$. The false positive PDF for a single delay measurement is assumed to be uniformly distributed as $f_{fp}(z_{\tau m,n}^{(j)}) = f_U(z_{\tau m,n}^{(j)}; 0, \tau_{\max})$. For a single AOA and AOD measurement, the false alarm PDF is assumed to be distributed as $f_{fp}(z_{\vartheta m,n}^{(j)}) = f_U(z_{\vartheta m,n}^{(j)}; -\pi, \pi)$ and $f_{fp}(z_{\varphi m,n}^{(j)}) = f_U(z_{\varphi m,n}^{(j)}; -\pi, \pi)$.

The mean number of PVA-related measurements $\mu_m(\mathbf{x}_{k,n}^{(j)}) \triangleq \mu_m(\boldsymbol{\psi}_{k,n}^{(j)})$ is well approximated as

$$\mu_m(\boldsymbol{\psi}_{k,n}^{(j)}) = \left(1 + \frac{N_{ny,\tau} \psi_{\tau,n}^{(j)}}{c T_s} + \frac{\psi_{\theta,n}^{(j)}}{N_{ny,\theta}} + \frac{\psi_{\varphi,n}^{(j)}}{N_{ny,\varphi}}\right) p_d \quad (16)$$

where p_d is the probability of the detection associated with the detection threshold γ of the CEDA, $N_{ny,\tau}$ is average number of components to be detected within one Nyquist sample, and $N_{ny,\theta}$ and $N_{ny,\varphi}$ are the average numbers of components within the respective Rayleigh resolutions.

C. New PVAs

Newly detected PVAs, i.e., actual VAs that generate a measurement for the first time, are modeled by a Poisson point process with mean μ_n and PDF $f_n(\bar{\mathbf{x}}_{m,n}^{(j)} | \mathbf{x}_n)$. Following [3], [26], newly detected VAs are represented by new PVA states $\bar{\mathbf{y}}_{m,n}^{(j)}$, $m \in \{1, \dots, M_n^{(j)}\}$, where each new PVA state corresponds to a measurement $\mathbf{z}_{m,n}^{(j)}$; $\bar{r}_{m,n}^{(j)} = 1$ implies that measurement $\mathbf{z}_{m,n}^{(j)}$ was generated by a newly detected VA. Since newly detected VAs can potentially produce more than one measurement, we use the multiple-measurement-to-feature probabilistic data association and define this mapping as introduced in [17], [22]. We also introduce the joint states $\bar{\mathbf{y}}_n^{(j)} \triangleq [\bar{\mathbf{y}}_{1,n}^{(j)} \dots \bar{\mathbf{y}}_{M_n^{(j)},n}^{(j)}]^T$ and $\bar{\mathbf{y}}_n \triangleq [\bar{\mathbf{y}}_n^{(1)T} \dots \bar{\mathbf{y}}_n^{(J)T}]^T$. The vector of all PVAs at time n is given by $\mathbf{y}_n \triangleq [\mathbf{y}_n^T \bar{\mathbf{y}}_n^T]^T$. Note that the total number of PVAs per PA is given by $K_n^{(j)} = K_{n-1}^{(j)} + M_n^{(j)}$.

Since new PVAs are introduced as new measurements are available at each time, the number of PVAs grows indefinitely. Thus, for feasible methods a suboptimal pruning step is employed that removes unlikely PVAs (see Section IV-F).

D. Association Vectors

SLAM is complicated by data association uncertainty meaning that it is unknown which measurement $\mathbf{z}_{m,n}^{(j)}$ originated from which VA. Furthermore, it is not known if a measurement did not originate from a PVA, i.e., it is a false positive measurement. Following [17], we use measurement-oriented association variables

$$\mathbf{b}_{m,n}^{(j)} \triangleq \begin{cases} k \in \{1, \dots, K_{n-1}^{(j)} + m\}, & \text{if measurement } m \text{ was} \\ & \text{generated by PVA } k \\ 0, & \text{otherwise} \end{cases}$$

and define the measurement-oriented association vector $\mathbf{b}_n^{(j)} = [\mathbf{b}_{1,n}^{(j)} \dots \mathbf{b}_{M_n^{(j)},n}^{(j)}]$. We also define $\mathbf{b}_n \triangleq [\mathbf{b}_n^{(1)T} \dots \mathbf{b}_n^{(J)T}]^T$.

E. Joint Posterior PDF

By using common assumptions [3], [26], and for fixed (observed) measurements $\mathbf{z}_{1:n}$, it can be shown that the joint posterior PDF of $\mathbf{x}_{1:n}$ ($\mathbf{x}_{1:n} \triangleq [\mathbf{x}_1^T \dots \mathbf{x}_n^T]^T$), $\mathbf{y}_{1:n}$, and $\mathbf{b}_{1:n}$, conditioned on $\mathbf{z}_{1:n}$ for all time steps $n' \in \{1, \dots, n\}$ is given by

$$\begin{aligned} & f(\mathbf{x}_{1:n}, \mathbf{y}_{1:n}, \mathbf{b}_{1:n} | \mathbf{z}_{1:n}) \\ & \propto f(\mathbf{x}_1) \prod_{j'=1}^J \prod_{k'=1}^{K_1^{(j')}} f(\mathbf{y}_{k',1}^{(j')}) \prod_{n'=2}^n f(\mathbf{x}_{n'} | \mathbf{x}_{n'-1}) \\ & \times \prod_{j=1}^J \left(\prod_{k=1}^{K_n^{(j)}} g(\mathbf{y}_{k,n}^{(j)} | \mathbf{y}_{k,n'-1}^{(j)}, \mathbf{x}_{n'-1}) \right. \\ & \times \left. \prod_{l=1}^{M_{n'}^{(j)}} q(\mathbf{x}_{n'}, \mathbf{y}_{k,n'}, b_{l,n'}^{(j)}; \mathbf{z}_{l,n'}^{(j)}) \right) \\ & \times \left(\prod_{m=1}^{M_{n'}^{(j)}} v(\mathbf{x}_{n'}, \bar{\mathbf{y}}_{m,n'}, b_{m,n'}^{(j)}; \mathbf{z}_{m,n'}^{(j)}) \right) \\ & \times \prod_{h=1}^{m-1} u(\mathbf{x}_{n'}, \bar{\mathbf{y}}_{m,n'}, b_{h,n'}^{(j)}; \mathbf{z}_{h,n'}^{(j)}) \end{aligned} \quad (17)$$

where $g(\mathbf{y}_{k,n}^{(j)} | \mathbf{y}_{k,n-1}^{(j)}, \mathbf{x}_{n-1})$, $q(\mathbf{x}_n, \mathbf{y}_{k,n}^{(j)}, b_{l,n}^{(j)}; \mathbf{z}_{l,n}^{(j)})$, $u(\mathbf{x}_n, \bar{\mathbf{y}}_{k,n}^{(j)}, b_{h,n}^{(j)}; \mathbf{z}_{h,n}^{(j)})$ and $v(\mathbf{x}_n, \bar{\mathbf{y}}_{m,n}^{(j)}, b_{m,n}^{(j)}; \mathbf{z}_{m,n}^{(j)})$ are explained in what follows. The *pseudo state-transition function* is given by

$$\begin{aligned} & g(\mathbf{y}_{k,n}^{(j)} | \mathbf{y}_{k,n-1}^{(j)}, \mathbf{x}_{n-1}) \\ & \triangleq \begin{cases} e^{-\mu_m(\mathbf{x}_{k,n}^{(j)})} f(\mathbf{x}_{k,n}^{(j)} | \mathbf{x}_{k,n-1}^{(j)}, \mathbf{r}_{k,n-1}^{(j)}), & \mathbf{r}_{k,n}^{(j)} = 1 \\ f(\mathbf{x}_{k,n}^{(j)} | \mathbf{x}_{k,n-1}^{(j)}, \mathbf{r}_{k,n-1}^{(j)}), & \mathbf{r}_{k,n}^{(j)} = 0 \end{cases} \end{aligned} \quad (18)$$

and the *pseudo prior distribution* as

$$f(\bar{\mathbf{y}}_{k,n}^{(j)} | \mathbf{x}_n) \triangleq \begin{cases} \mu_n f_n(\bar{\mathbf{x}}_{k,n}^{(j)} | \mathbf{x}_n) e^{-\mu_m(\bar{\mathbf{x}}_{k,n}^{(j)})}, & \bar{r}_{k,n}^{(j)} = 1 \\ f_d(\bar{\mathbf{x}}_{k,n}^{(j)}), & \bar{r}_{k,n}^{(j)} = 0. \end{cases} \quad (19)$$

The *pseudo likelihood functions* related to legacy PVAs for $k \in \mathcal{K}_{n-1}^{(j)}$ $q(\mathbf{x}_n, \mathbf{y}_{k,n}^{(j)}, b_{l,n}^{(j)}; \mathbf{z}_{l,n}^{(j)}) = q(\mathbf{x}_n, \mathbf{x}_{k,n}^{(j)}, \mathbf{r}_{k,n}^{(j)}, b_{l,n}^{(j)}; \mathbf{z}_{l,n}^{(j)})$ is given by

$$\begin{aligned} & q(\mathbf{x}_n, \mathbf{x}_{k,n}^{(j)}, 1, b_{l,n}^{(j)}; \mathbf{z}_{l,n}^{(j)}) \\ & \triangleq \begin{cases} \frac{\mu_m(\mathbf{x}_{k,n}^{(j)}) f(\mathbf{z}_{l,n}^{(j)} | \mathbf{p}_n, \mathbf{x}_{k,n}^{(j)})}{\mu_{fp} f_{fp}(\mathbf{z}_{l,n}^{(j)})}, & b_{l,n}^{(j)} = k \\ 1, & b_{l,n}^{(j)} \neq k \end{cases} \end{aligned} \quad (20)$$

and $q(\mathbf{x}_n, \mathbf{x}_{k,n}^{(j)}, 0, b_{l,n}^{(j)}; \mathbf{z}_{l,n}^{(j)}) \triangleq 1 - \delta(b_{l,n}^{(j)} - k)$. The *pseudo likelihood functions* related to a new PVA (with $k \in \mathcal{M}_n^{(j)} \setminus m$) $u(\mathbf{x}_n, \bar{\mathbf{y}}_{k,n}^{(j)}, b_{h,n}^{(j)}; \mathbf{z}_{h,n}^{(j)}) = u(\mathbf{x}_n, \bar{\mathbf{x}}_{k,n}^{(j)}, \bar{r}_k^{(j)}, b_{h,n}^{(j)}; \mathbf{z}_{h,n}^{(j)})$, where $h \in \{1, \dots, m-1\}$ is given by

$$\begin{aligned} & u(\mathbf{x}_n, \bar{\mathbf{x}}_{k,n}^{(j)}, 1, b_{h,n}^{(j)}; \mathbf{z}_{h,n}^{(j)}) \\ & \triangleq \begin{cases} \frac{f(\bar{\mathbf{y}}_{k,n}^{(j)} | \mathbf{x}_n) \mu_m(\bar{\mathbf{x}}_{k,n}^{(j)}) f(\mathbf{z}_{h,n}^{(j)} | \mathbf{p}_n, \bar{\mathbf{x}}_{k,n}^{(j)})}{\mu_{fp} f_{fp}(\mathbf{z}_{h,n}^{(j)})}, & b_{h,n}^{(j)} = K_{n-1}^{(j)} + k \\ 1, & b_{h,n}^{(j)} \neq K_{n-1}^{(j)} + k \end{cases} \end{aligned} \quad (21)$$

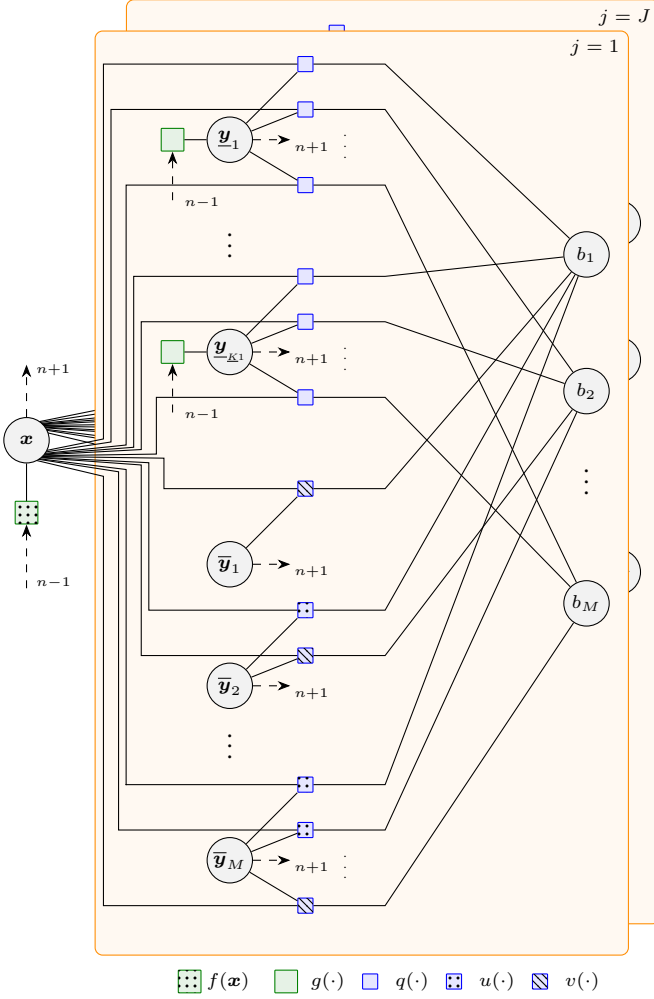


Fig. 2. Factor graph for proposed algorithm. At MP iteration p , we use the following short hand notation: $f(\mathbf{x}) \triangleq f(\mathbf{x}_n | \mathbf{z}_{1:n-1})$, $g(\cdot)$, $q(\cdot)$, $u(\cdot)$ and $v(\cdot)$ corresponds to (18), (20), (21), (22), respectively. The time evolution of the agent state and VAs is indicated with dashed arrows.

and $u(\mathbf{x}_n, \bar{\mathbf{x}}_{k,n}^{(j)}, 0, b_{h,n}^{(j)}; \mathbf{z}_{h,n}^{(j)}) \triangleq 1 - \delta(b_{h,n}^{(j)} - (K_{n-1}^{(j)} + k))$, whereas for $k = m$ as $v(\mathbf{x}_n, \bar{\mathbf{y}}_m^{(j)}, b_{m,n}^{(j)}; \mathbf{z}_{m,n}^{(j)}) = v(\mathbf{x}_n, \bar{\mathbf{x}}_{m,n}^{(j)}, \bar{\mathbf{r}}_{m,n}^{(j)}, b_{m,n}^{(j)}; \mathbf{z}_{m,n}^{(j)})$ is given by

$$v(\mathbf{x}_n, \bar{\mathbf{x}}_{m,n}^{(j)}, 1, b_{m,n}^{(j)}; \mathbf{z}_{m,n}^{(j)}) \triangleq \begin{cases} \frac{f(\bar{\mathbf{y}}_{m,n}^{(j)} | \mathbf{x}_n) \mu_m(\bar{\mathbf{x}}_{m,n}^{(j)}) f(\mathbf{z}_{m,n}^{(j)} | \mathbf{p}_n, \bar{\mathbf{x}}_{m,n}^{(j)})}{\mu_{ip} f_{ip}(\mathbf{z}_{m,n}^{(j)})}, & b_{m,n}^{(j)} = K_{n-1}^{(j)} + m \\ 0, & b_{m,n}^{(j)} \neq K_{n-1}^{(j)} + m \end{cases} \quad (22)$$

and $v(\mathbf{x}_n, \bar{\mathbf{x}}_{m,n}^{(j)}, 0, b_{m,n}^{(j)}; \mathbf{z}_{m,n}^{(j)}) \triangleq 1 - \delta(b_{m,n}^{(j)} - (K_{n-1}^{(j)} + m))$. The factor graph representing the factorization (17) is shown in Fig. 2. The proposed message passing is similar to [20].

F. Detection of PVAs and State Estimation

At each time n and for each PA j , the CEDA provides the currently observed measurement vector $\mathbf{z}_n^{(j)}$, with fixed $M_n^{(j)}$, according to Section III-A. We aim to estimate all states using all available measurements $\mathbf{z}_{1:n}$ from all PAs up to time n . We

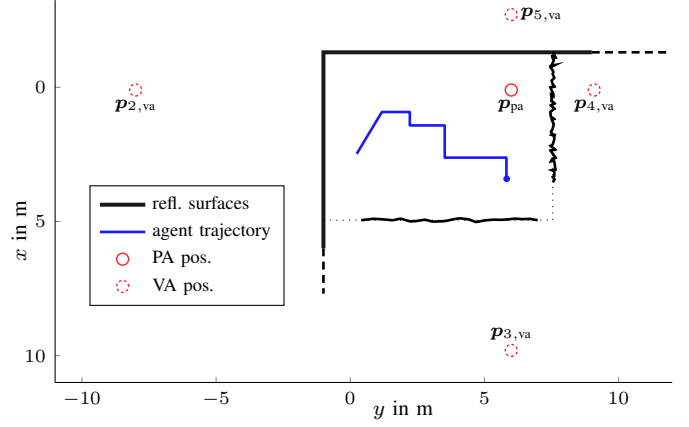


Fig. 3. Considered scenario for performance evaluation. Perfect reflectors are indicated with straight lines and rough surfaces with wavy lines.

calculate estimates of the agent state \mathbf{x}_n by using the minimum mean-square error (MMSE) estimator [30, Ch. 4], i.e.,

$$\mathbf{x}_n^{\text{MMSE}} \triangleq \int \mathbf{x}_n f(\mathbf{x}_n | \mathbf{z}_{1:n}) d\mathbf{x}_n \quad (23)$$

The map of the environment is represented by reflective surfaces described by PVAs. Therefore, the state $\mathbf{x}_{k,n}^{(j)}$ of the detected PVAs $k \in \{1, \dots, K_n^{(j)}\}$ must be estimated. This relies on the marginal posterior existence probabilities $p(r_{k,n}^{(j)} = 1 | \mathbf{z}_{1:n}) = \int f(\mathbf{x}_{k,n}^{(j)}, r_{k,n}^{(j)} = 1 | \mathbf{z}_{1:n}) d\mathbf{x}_{k,n}^{(j)}$ and the marginal posterior PDFs $f(\mathbf{x}_{k,n}^{(j)} | r_{k,n}^{(j)} = 1, \mathbf{z}_{1:n}) = f(\mathbf{x}_{k,n}^{(j)}, r_{k,n}^{(j)} = 1 | \mathbf{z}_{1:n}) / p(r_{k,n}^{(j)} = 1 | \mathbf{z}_{1:n})$. A PVA k is declared to exist if $p(r_{k,n}^{(j)} = 1 | \mathbf{z}_{1:n}) > p_{\text{cf}}$, where p_{cf} is a confirmation threshold [30, Ch. 2]. To avoid that the number of PVA states grows indefinitely, PVA states with $p(r_{k,n}^{(j)} = 1 | \mathbf{z}_{1:n})$ below a threshold p_{pr} are removed from the state space (“pruned”). The number $\hat{K}_n^{(j)}$ of PVA states that are considered to exist is the estimate of the total number $L_n^{(j)}$ of VAs visible at time n . For existing PVAs, an estimate of its state $\mathbf{x}_{k,n}^{(j)}$ can again be calculated by the MMSE

$$\mathbf{x}_{k,n}^{(j)\text{MMSE}} \triangleq \int \mathbf{x}_{k,n}^{(j)} f(\mathbf{x}_{k,n}^{(j)} | r_{k,n}^{(j)} = 1, \mathbf{z}_{1:n}) d\mathbf{x}_{k,n}^{(j)} \quad (24)$$

where $\mathbf{x}_{k,n}^{(j)\text{MMSE}} = [\mathbf{p}_{k,n}^{(j)\text{MMSE}}, \boldsymbol{\psi}_{k,n}^{(j)\text{MMSE}}]^T$. The calculation of $f(\mathbf{x}_n | \mathbf{z}_{1:n})$, $p(r_{k,n} = 1 | \mathbf{z})$, and $f(\mathbf{x}_{k,n}^{(j)} | r_{k,n}^{(j)} = 1, \mathbf{z}_{1:n})$ from the joint posterior $f(\mathbf{x}_{1:n}, \mathbf{y}_{1:n}, \mathbf{b}_{1:n} | \mathbf{z}_{1:n})$ by direct marginalization is not feasible. By performing sequential particle-based message passing (MP) [3], [26], [31] using the SPA rules [32] on the factor graph in Fig. 2, approximations (“beliefs”) $b(\mathbf{x}_n)$ and $b(\mathbf{y}_{k,n}^{(j)})$ of the marginal posterior PDFs $f(\mathbf{x}_n | \mathbf{z}_{1:n})$, $p(r_{k,n}^{(j)} = 1 | \mathbf{z}_{1:n})$, and $f(\mathbf{x}_{k,n}^{(j)} | r_{k,n}^{(j)} = 1, \mathbf{z}_{1:n})$ can be obtained in an efficient way for the agent state as well as all legacy and new PVA states.

V. NUMERICAL RESULTS

We consider an indoor scenario shown in Fig. 3. The scenario consists of one PA at position $\mathbf{p}_{\text{pa}}^{(1)} = [0.1 \ 6]^T$ and four reflective surfaces, i.e., 4 VAs. The agent moves along a track which is observed for 300 time instances n with observation period $\Delta T = 1$ s.

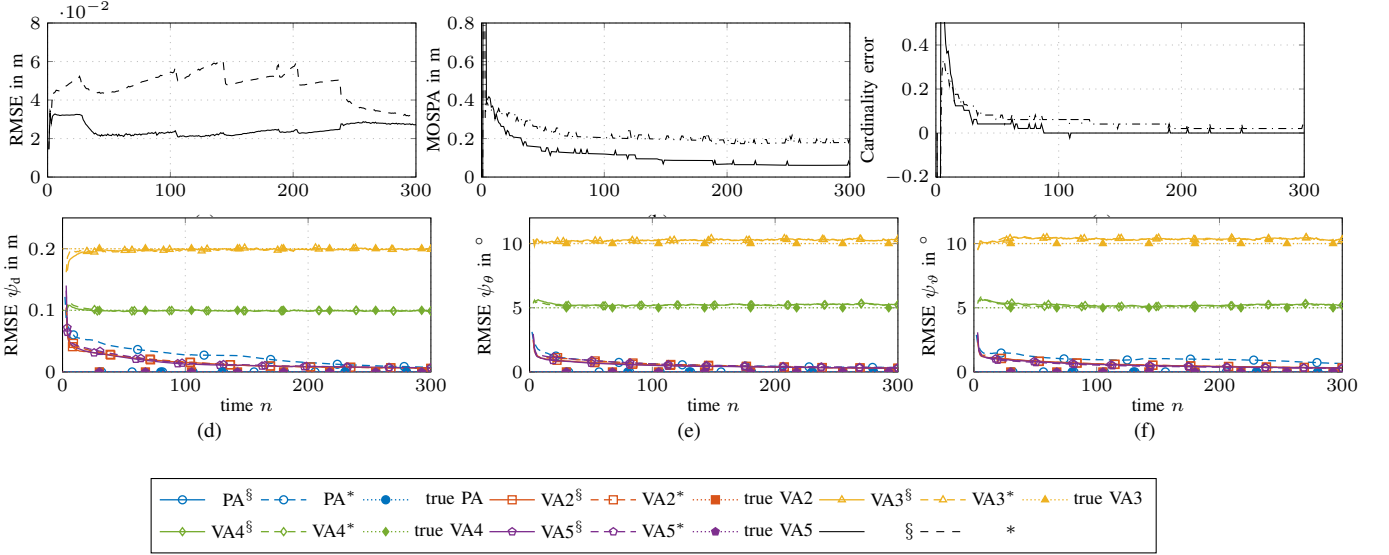


Fig. 4. Results for converged simulation runs. (a) shows the RMSE of the agent position over the whole track. (b) and (c) present the MOSPA and the cardinality error. (d) - (f) show the RMSE of the dispersion parameters. The legend is explained in what follows. The word *true* and dotted lines indicate the true dispersion parameters for each PA or VA. § and solid lines correspond to unknown VA dispersion parameters but known PA dispersion parameters. * and dashed lines indicate unknown dispersion parameters.

Measurements are generated according to the proposed system model in Section IV-B and to the scenario shown in Fig. 3. The distances of the main components are calculated based on the PA and the corresponding VAs positions as well as the agent positions (see Section III). The signal-to-noise-ratio (SNR) is set to 40 dB at an LOS distance of 1 m. The amplitudes of the main-components (LOS component and the MPCs) are calculated using a free-space path loss model and an additional attenuation of 3 dB for each reflection at a surface. The sub-components are generated with a constant amplitude attenuation $\beta_{l,i,n} = 0.9$ for all i and for all n and fixed dispersion parameters $\psi_{\tau,l,n} = \psi_{\tau,l} = \psi_{d,l}/c$, $\psi_{\theta,k,n} = \psi_{\theta,k}$, and $\psi_{\vartheta,k,n} = \psi_{\vartheta,k}$ for all n . We define $N_{ny} = 4$, $N_{ny,\theta} = N_{ny,\vartheta} = 2$ and $p_d = 0.98$. In addition false positive measurements are generated according to the model in Section IV-B with a mean number of $\mu_{fp} = 5$. For the calculation of the measurement variances, we assume a 3-dB system bandwidth of $B = 500$ MHz for some known transmit signal spectrum for a carrier frequency of $f_c = 6$ GHz. The arrays employed at agent and PA are of identical geometry with $H = H^{(j)} = 9$ antenna elements in (known) uniform rectangular array (URA)-configuration spaced at $\lambda/2$, where $\lambda = c/f_c$ is the carrier wavelength. We use 10^5 particles. The particles for the initial agent state are drawn from a 4-D uniform distribution with center $\mathbf{x}_0 = [\mathbf{p}_0^T \ 0 \ 0]^T$, where \mathbf{p}_0 is the starting position of the actual agent track, and the support of each position component about the respective center is given by $[-0.1 \text{ m}, 0.1 \text{ m}]$ and of each velocity component is given by $[-0.01 \text{ m/s}, 0.01 \text{ m/s}]$. At time $n = 0$, the number of VAs is 0, i.e., no prior map information is available. The prior distribution for new PVA states $f_n(\bar{\mathbf{x}}_{m,n}^{(j)} | \mathbf{x}_n)$ is uniform on the square region given by $[-15 \text{ m}, 15 \text{ m}] \times [-15 \text{ m}, 15 \text{ m}]$ around the center of the floor plan shown in Fig. 3 and the mean number of new PVAs at time n is $\mu_n = 0.01$. The probability of survival is $p_s = 0.999$. The confirmation threshold as

TABLE I
DISPERSION PARAMETER SETTINGS

	PA	VA1	VA2	VA3	VA4
ψ_d	0 m	0 m	0.2 m	0.1 m	0 m
ψ_θ	0°	0°	10°	5°	0°
ψ_ϑ	0°	0°	10°	5°	0°

well as the pruning threshold are given as $p_{cf} = 0.5$ and $p_{pr} = 10^{-3}$, respectively. For the sake of numerical stability, we introduce a small amount of regularization noise to the VA state $\mathbf{p}_{k,va}$ at each time step n , i.e., $\underline{\mathbf{p}}_{k,va}^{(j)} = \mathbf{p}_{k,va}^{(j)} + \boldsymbol{\omega}_k$, where $\boldsymbol{\omega}_k$ is iid across k , zero-mean, and Gaussian with covariance matrix $\sigma_a^2 \mathbf{I}_2$ and $\sigma_a = 10^{-3}$ m. The state transition variances are set as $\sigma_w = 10^{-3} \text{ m/s}^2$, $q_\tau = q_\theta = q_\vartheta = 10^3$ [17], [28]. The performance is measured in terms of the RMSE of the agent position and the dispersion parameters as well as the optimal subpattern assignment (OSPA) error [33] of all VAs with cutoff parameter and order set to 5 m and 2, respectively. The MOSPA errors and RMSEs of each unknown variable are obtained by averaging over all converged simulation runs.

Experiment: For the investigation of the proposed method, we define for each surface an individual roughness as shown in Fig. 3. This is captured by individual dispersion parameter settings as given in Table I. We performed 100 simulation runs. In each simulation run, we generated noisy measurements $\mathbf{z}_{m,n}^{(j)}$ according to the measurement model proposed in Section IV-B. In the case $\psi_k = 0$ only main-component measurements are generated, which is equivalent to the system model in [8]. The results are summarized in Fig. 4. We investigated the impact of two different settings on the estimation performance. The first one assumes the dispersion parameters of the PA as known and of the VAs as unknown. The second one assumes all dispersion parameters as unknown. The RMSE of the agent positions is shown in Fig. 4a. Assuming known dispersion parameters for the PA results in the smallest RMSE. The results show that estimating the dispersion parameters

comes at the cost of localization accuracy. Fig. 4b and 4c show the MOSPA error and its mean cardinality error contributions, respectively. After a few time steps, the number of VAs is estimated correctly, hence the only significant contribution in the MOSPA are the positioning errors of the VAs. It shows a slight performance gap between unknown and known PA dispersion parameters due to the same reasons as mentioned above. The RMSEs of the dispersion parameters are presented in Fig. 4d, 4e and 4f. The true values are indicated with dashed lines in the same color. The results show that the dispersion parameters are well estimated and converge to the true value. For dispersion parameters equal to zero, the convergence is much slower. This is due to the fact that for a single measurement, there is a model mismatch in the likelihood. This could lead to a biased estimate at the beginning, which reduces to zero over time as indicated by the results. In addition, knowing the PA dispersion parameters has no significant impact on the estimation accuracy of the other dispersion parameters. For the unknown PA dispersion parameters, we observe a slightly slower convergence to zero. We assume that this is caused by the smaller measurement variance due to the higher amplitude of the LOS path.

VI. CONCLUSIONS

We have proposed a new MP-SLAM for non-ideal reflective surfaces in MIMO wireless communication systems where single- or multiple-measurements can be generated by a single environment feature (i.e., a single VA). By introducing individual dispersion parameters for each PA and VA, the proposed method fuses the information contained in ideal and non-ideal reflective surfaces. We demonstrated that the proposed algorithm can robustly and jointly estimate the position and dispersion extents of ideal and non-ideal reflective in a challenging scenario involving different types of surfaces. Possible directions for future research include incorporating multiple-measurements-to-feature data association into the MVA-based SLAM method.

REFERENCES

- [1] E. Leitingner, P. Meissner, C. Rudisser, G. Dumphart, and K. Witrisal, "Evaluation of position-related information in multipath components for indoor positioning," *IEEE J. Sel. Areas Commun.*, vol. 33, no. 11, pp. 2313–2328, Nov. 2015.
- [2] K. Witrisal, P. Meissner, E. Leitingner, Y. Shen, C. Gustafson, F. Tufvesson, K. Haneda, D. Dardari, A. F. Molisch, A. Conti, and M. Z. Win, "High-accuracy localization for assisted living: 5G systems will turn multipath channels from foe to friend," *IEEE Signal Process. Mag.*, vol. 33, no. 2, pp. 59–70, Mar. 2016.
- [3] E. Leitingner, F. Meyer, F. Hlawatsch, K. Witrisal, F. Tufvesson, and M. Z. Win, "A belief propagation algorithm for multipath-based SLAM," *IEEE Trans. Wireless Commun.*, vol. 18, no. 12, pp. 5613–5629, Dec. 2019.
- [4] R. Mendrzik, F. Meyer, G. Bauch, and M. Z. Win, "Enabling situational awareness in millimeter wave massive MIMO systems," *IEEE J. Sel. Topics Signal Process.*, vol. 13, no. 5, pp. 1196–1211, Sep. 2019.
- [5] C. Gentner, W. Jost, T. and Wang, S. Zhang, A. Dammann, and U. C. Fiebig, "Multipath assisted positioning with simultaneous localization and mapping," *IEEE Trans. Wireless Commun.*, vol. 15, no. 9, pp. 6104–6117, Sept. 2016.
- [6] H. Durrant-Whyte and T. Bailey, "Simultaneous localization and mapping: Part I," *IEEE Robot. Autom. Mag.*, vol. 13, no. 2, pp. 99–110, June 2006.
- [7] M. Dissanayake, P. Newman, S. Clark, H. Durrant-Whyte, and M. Csorba, "A solution to the simultaneous localization and map building (SLAM) problem," *IEEE Trans. Robot. Autom.*, vol. 17, no. 3, pp. 229–241, June 2001.
- [8] E. Leitingner, S. Grebien, and K. Witrisal, "Multipath-based SLAM exploiting AoA and amplitude information," in *Proc. IEEE ICCW-19*, Shanghai, China, May 2019, pp. 1–7.
- [9] H. Kim, K. Granström, L. Gao, G. Battistelli, S. Kim, and H. Wymeersch, "5G mmWave cooperative positioning and mapping using multi-model PHD filter and map fusion," *IEEE Trans. Wireless Commun.*, vol. 19, no. 6, pp. 3782–3795, Mar. 2020.
- [10] H. Kim, K. Granström, L. Svensson, S. Kim, and H. Wymeersch, "PMBM-based SLAM filters in 5G mmWave vehicular networks," *IEEE Trans. Veh. Technol.*, pp. 1–1, May 2022.
- [11] E. Leitingner and F. Meyer, "Data fusion for multipath-based SLAM," in *Proc. Asilomar-20*, Pacific Grove, CA, USA, Oct. 2020, pp. 934–939.
- [12] E. Leitingner, A. Venus, B. Teague, and F. Meyer, "Data fusion for multipath-based SLAM: Combining information from multiple propagation paths," *IEEE Trans. Signal Process.*, vol. 71, pp. 4011–4028, Sep. 2023.
- [13] D. Shutin, W. Wang, and T. Jost, "Incremental sparse Bayesian learning for parameter estimation of superimposed signals," in *Proc. SAMPTA-2013*, no. 1, Sept. 2013, pp. 6–9.
- [14] M. A. Badiu, T. L. Hansen, and B. H. Fleury, "Variational Bayesian inference of line spectra," *IEEE Trans. Signal Process.*, vol. 65, no. 9, pp. 2247–2261, May 2017.
- [15] X. Li, E. Leitingner, A. Venus, and F. Tufvesson, "Sequential detection and estimation of multipath channel parameters using belief propagation," *IEEE Trans. Wireless Commun.*, vol. 21, no. 10, pp. 8385–8402, Apr. 2022.
- [16] S. Grebien, E. Leitingner, K. Witrisal, and B. H. Fleury, "Super-resolution estimation of UWB channels including the dense component – An SBL-inspired approach," *IEEE Trans. Wireless Commun.*, 2024.
- [17] F. Meyer and J. L. Williams, "Scalable detection and tracking of geometric extended objects," *IEEE Trans. Signal Process.*, vol. 69, pp. 6283–6298, Oct. 2021.
- [18] J. Kulmer, F. Wen, N. Garcia, H. Wymeersch, and K. Witrisal, "Impact of rough surface scattering on stochastic multipath component models," in *Proc. IEEE PIMRC 2018*, Bologna, Italy, Dec. 2018, pp. 1410–1416.
- [19] F. Wen, J. Kulmer, K. Witrisal, and H. Wymeersch, "5G positioning and mapping with diffuse multipath," *IEEE Trans. Wireless Commun.*, vol. 20, no. 2, pp. 1164–1174, 2021.
- [20] L. Wielandner, A. Venus, T. Wilding, and E. Leitingner, "Multipath-based SLAM for non-ideal reflective surfaces exploiting multiple-measurement data association," *arXiv preprint arXiv:2304.05680*, 2023.
- [21] —, "Multipath-based SLAM with multiple-measurement data association," in *Proc. Fusion-23*, Charleston, USA, Jul. 2023, pp. 1–8.
- [22] F. Meyer and J. L. Williams, "Scalable detection and tracking of extended objects," in *Proc. ICASSP 2020*, Barcelona, Spain, May 2020, pp. 8916–8920.
- [23] S. M. Kay, *Fundamentals of Statistical Signal Processing: Detection Theory*. Upper Saddle River, NJ, USA: Prentice Hall, 1998.
- [24] A. Saleh and R. Valenzuela, "A statistical model for indoor multipath propagation," *IEEE J. Sel. Areas Commun.*, vol. 5, no. 2, pp. 128–137, Feb. 1987.
- [25] T. Pedersen, "Modeling of path arrival rate for in-room radio channels with directive antennas," *IEEE Trans. Antennas Propag.*, vol. 66, no. 9, pp. 4791–4805, 2018.
- [26] F. Meyer, T. Kropfreiter, J. L. Williams, R. Lau, F. Hlawatsch, P. Braca, and M. Z. Win, "Message passing algorithms for scalable multitarget tracking," *Proc. IEEE*, vol. 106, no. 2, pp. 221–259, Feb. 2018.
- [27] Y. Bar-Shalom, T. Kirubarajan, and X.-R. Li, *Estimation with Applications to Tracking and Navigation*. New York, NY, USA: John Wiley & Sons, Inc., 2002.
- [28] J. W. Koch, "Bayesian approach to extended object and cluster tracking using random matrices," *IEEE Trans. Aerosp. Electron. Syst.*, vol. 44, no. 3, pp. 1042–1059, Jul. 2008.
- [29] T. Wilding, S. Grebien, E. Leitingner, U. Mühlmann, and K. Witrisal, "Single-anchor, multipath-assisted indoor positioning with aliased antenna arrays," in *Proc. Asilomar-18*, Pacific Grove, CA, USA, Oct. 2018, pp. 525–531.
- [30] H. V. Poor, *An Introduction to Signal Detection and Estimation*, 2nd ed. New York: Springer-Verlag, 1994.
- [31] F. Meyer, O. Hlinka, H. Wymeersch, E. Riegler, and F. Hlawatsch, "Distributed localization and tracking of mobile networks including noncooperative objects," vol. 2, no. 1, pp. 57–71, Mar. 2016.
- [32] F. Kschischang, B. Frey, and H.-A. Loeliger, "Factor graphs and the sum-product algorithm," *IEEE Trans. Inf. Theory*, vol. 47, no. 2, pp. 498–519, Feb. 2001.

- [33] D. Schuhmacher, B.-T. Vo, and B.-N. Vo, "A consistent metric for performance evaluation of multi-object filters," *IEEE Trans. Signal Process.*, vol. 56, no. 8, pp. 3447–3457, Aug. 2008.